Journal of Power Sources 231 (2013) 44–49

Contents lists available at SciVerse ScienceDirect

Journal of Power Sources

journal homepage: www.elsevier.com/locate/jpowsour

Surface modification of $Li_{1.2}Mn_{0.54}Co_{0.13}Ni_{0.13}O_2$ with conducting polypyrrole

Chengren Wu [a,b,c], Xiangpeng Fang [a], Xianwei Guo [a], Ya Mao [a], Jun Ma [a], Changchun Zhao [c], Zhaoxiang Wang [a,*], Liquan Chen [a]

[a] Laboratory for Solid State Ionics, Institute of Physics, Chinese Academy of Sciences, PO Box 603, Beijing 100190, China
[b] NingDe Amperex Technology Limited, Ningde, Fujian 352100, China
[c] School of Science, China University of Geosciences, Beijing 100083, China

HIGHLIGHTS

- $Li_{1.2}Mn_{0.54}Co_{0.13}Ni_{0.13}O_2$ (LMO) is surface-coated with conducting polypyrrole (PPy).
- Coating improves the initial coulombic efficiency and capacity retention of LMO.
- SEI layer is observed and its composition recognized on PPy-coated LMO at 4.8 V.

ARTICLE INFO

Article history:
Received 28 March 2012
Received in revised form
10 August 2012
Accepted 28 November 2012
Available online 26 December 2012

Keywords>:
Lithium-ion batteries
Layered oxide cathode materials
Polypyrrole
Surface modification
Electrochemical performance

ABSTRACT

The lithium-rich solid solutions between layer-structured Li_2MO_3 (M = Mn, Zr, Ti) and $LiM'O_2$ (M′ = $Mn_{0.5}Ni_{0.5}$, $Mn_{0.33}Co_{0.33}Ni_{0.33}$, Co, *etc.*) are attractive cathode materials for lithium ion batteries with high specific energies. However, these solid solutions suffer from low coulombic efficiency due to the loss of oxygen in the form of Li_2O and electrolyte decomposition at high potentials in the initial cycle and poor cyclability due to decreased number of sites for lithium ion insertion/extraction in the subsequent cycles. In addition, the presence of a solid electrolyte interphase layer on these solid solutions is still in argument. In this work, $Li_{1.2}Mn_{0.54}Co_{0.13}Ni_{0.13}O_2$ ($0.5Li_2MnO_3 \cdot 0.5LiMn_{0.33}Co_{0.33}Ni_{0.33}O_2$) is prepared by Pechini method and coated with conducting polypyrrole (PPy). The physical characterization (XRD, SEM, HRTEM, FTIR) and electrochemical evaluation (EIS, CV and galvanostatic cycling) demonstrate the effectiveness of the surface modification on improving the electrochemical performances of the solid solution and the presence of a solid electrolyte interphase layer on the charged PPy-modified material.

1. Introduction

Lithium ion batteries (LIBs) are attractive rechargeable batteries due to their high energy density [1]. However, the low available specific capacity of the traditional cathode materials such as $LiCoO_2$, $LiMn_2O_4$, and $LiFePO_4$ is becoming a bottleneck to the increase of the energy densities of the LIBs for electric vehicles that are expected to drive 300 miles between two charges. The solid solutions of layer-structured Li_2MO_3 (M = Mn, Zr, Ti) and $LiM'O_2$ (M′ = $Mn_{0.5}Ni_{0.5}$, $Mn_{0.33}Co_{0.33}Ni_{0.33}$, Co, *etc.*) is a promising alternate cathode material for high energy density LIBs because they exhibit much higher capacity (>200 mAh g^{-1}) as well as lower cost, higher safety and thermal stability [2,3]. For example, layer-structured oxides $(1-z)Li[Li_{1/3}Mn_{2/3}]O_2 \cdot zLi[Mn_{0.5-y}Ni_{0.5-y}Co_{2y}]O_2$ (y = 1/6, and $0.25 \le z \le 0.75$) [4–6] deliver capacities as high as 250 mAh g^{-1} when charged to 4.8 V. However, the irreversible capacity loss of these oxides is high in the initial cycle [7] and their cyclability is poor because the lithium is extracted in the form of Li_2O at high potentials. That is, the lithium extraction is accompanied with the elimination of oxygen vacancies during the first charge, resulting in a lowered number of Li^+ ion insertion sites for the subsequent cycles. Moreover, the poor rate performance of these materials pushes them farther away from commercialization due to the low electronic conductivity induced by the insulating Li_2MnO_3 component [8]. These drawbacks become impediment in their applications in power-type LIBs.

Surface modification has been proved an effective method in reducing the irreversible capacity of the cathode materials in the initial cycle by suppressing the elimination of oxygen ion vacancies and the reaction between the active material and the electrolyte at

* Corresponding author. Tel./fax: +86 10 82649050.
E-mail address: zxwang@iphy.ac.cn (Z. Wang).

0378-7753/$ – see front matter © 2012 Elsevier B.V. All rights reserved.
http://dx.doi.org/10.1016/j.jpowsour.2012.11.138

high potentials. $AlPO_4$ [7], carbon [8], Al_2O_3 [9], Al [10], AlF_3 [11], TiO_2 [12], *etc.* have been employed as coating materials for surface modification of lithium-rich cathode materials to improve their cyclability and thermal stability at high cutoff charge potentials. Recently, the high conductivity and elasticity of polypyrrole (PPy) were explored to improve the rate performance and/or cycling stability of low-conductivity electrode materials such as Si [13], Co_3O_4 [14], and $LiFePO_4$ [15]. Meanwhile, PPy was also used to separate the electrolyte from the highly reactive cathode materials at high potentials such as LiV_3O_8 [16], $LiMn_2O_4/Li_xV_2O_5$ [17] and $LiMn_{0.33}Co_{0.33}Ni_{0.33}O_2$ [18]. However, the cutoff charge potentials of all these materials are ≤4.6 V *vs.* Li^+/Li. The impacts of PPy coating on the electrochemical performance of the Li-rich solid solutions are unknown.

The presence of solid electrolyte interphase (SEI) layer has become a common sense on the anode materials discharged below 0.75 V and on most of the cathode materials charged above 4.2 V *vs.* Li^+/Li. However, the existence and composition of the SEI layer on these Li-rich solid solutions are still unknown. Liu et al. [8] claimed that an SEI layer is formed on the Li-rich electrode materials when charged to 4.8 V. However, they did not provide any experimental evidence.

In this study, $Li_{1.2}Mn_{0.54}Co_{0.13}Ni_{0.13}O_2$ was prepared and cycled between 2.0 and 4.8 V *vs.* Li^+/Li. Its initial coulombic efficiency and cycling stability were characterized and compared before and after PPy surface modification. Evidence of the formation of the SEI on 4.8 V charged $Li_{1.2}Mn_{0.54}Co_{0.13}Ni_{0.13}O_2$ was obtained by FTIR and TEM.

2. Experimental

Layer-structured $Li_{1.2}Mn_{0.54}Co_{0.13}Ni_{0.13}O_2$ was synthesized by the Pechini method. Stoichiometric amounts (with 5% excess lithium) of $LiNO_3$, $Ni(NO_3)_2\cdot 6H_2O$, $Co(NO_3)_2\cdot 6H_2O$ and $Mn(NO_3)_2\cdot 4H_2O$ were dissolved in de-ionized water. The resulting solution was added into a mixture of ethylene glycol and citric acid (molar ratio 1:4). The mixed solution was evaporated at 135 °C for 6 h during continuous stirring. The dried powder was at first calcined at 300 °C for 5 h and then calcined at 800 °C for 12 h in air before cooled down to room temperature.

PPy surface modification (2.0 wt%) was carried out by chemical oxidation polymerization method. The required amount of pyrrole monomer (AR, 99%), toluene-4 solphomic acid sodium salt (CP, 98%) as doping agent and $Li_{1.2}Mn_{0.54}Co_{0.13}Ni_{0.13}O_2$ were ultrasonically dispersed in de-ionized water. Then the aqueous solution of $FeCl_3$ (AR, 99%) was slowly added as an oxidizing agent. The mixture was then magnetically stirred for 6 h in an ice/water bath to complete the polymerization reaction. The final product was filtered, washed with de-ionized water for several times, and finally dried at 80 °C for overnight.

The working electrode was prepared by mixing 80 wt% active materials, 10 wt% carbon black, and 10 wt% polyvinylidene fluorides (PVDF) and vigorously stirred in NMP to form slurry. The slurry was spread on an Al foil and dried at 100 °C in vacuum for 12 h. Two-electrode button cells (half cells) were assembled in an argon-filled glove box using fresh lithium foil as the counter electrode, 1 M $LiPF_6$ dissolved in a mixture of ethylene carbonate (EC) and dimethyl carbonate (DMC) (1:1 by volume) as the electrolyte, and Celgard 2300 as the separator. The charge/discharge measurements were carried out on a Land BT2000 battery tester (Wuhan, China). Electrochemical performances were evaluated between 2.0 and 4.8 V at 12.5 mA g^{-1} (~C/20). Electrochemical impedance spectroscopic (EIS) measurements were carried out between 5 mHz and 4 MHz on an M6e electrochemical workstation (Zennium, Germany). Cyclic voltammetry was carried out between 2.0 and 4.8 V at 0.1 mV s^{-1} scanning rate on an automatic battery tester (Autolab, PGSTAT128N).

The contents of Li, Ni, Mn, Co in the as-prepared (AP-LMCN) and PPy-coated (PPy-LMCN) $Li_{1.2}Mn_{0.54}Co_{0.13}Ni_{0.13}O_2$ were determined on IRIS Intrepid II (Thermo Scientific, America) inductively coupled plasma-atomic emission spectrometer (ICP-AES). The crystalline structures of the AP-LMCN and PPy-LMCN were analyzed on X'Pert Pro MPD X-ray diffracter (Philips, Holland) operated at 40 kV. The electrode sheets of the AP-LMCN and PPy-LMCN were rinsed with DMC to remove the residual electrolyte after the half cell was galvanostatically charged to 4.8 V *vs.* Li^+/Li. The FTIR spectra of these sheets were recorded on a VERTEX 70 V FTIR spectrometer (Bruker, Germany). The morphology of the electrode material was observed on a Hitachi S-4800 scanning electron microscope. To investigate the microstructure of the material, high-resolution transmission electron microscopy (HRTEM; JEOL 2010) was conducted.

3. Results and discussion

Fig. 1 compares the XRD patterns of the AP-LMCN and PPy-LMCN. Most of the XRD diffractions of both materials can be indexed to the α-$NaFeO_2$ structure. The weak superstructure of the (020) and (110) diffractions between 20 and 25° (2θ) belongs to the $Li[Li_{1/3}Mn_{2/3}]O_2$ structure in the solid solution [19]. The XRD pattern of the PPy-LMCN is actually identical to that of the AP-LMCN. No significant lattice parameter differences could be recognized between them. These indicate that the AP-LMCN is pure and no other impurities were formed or introduced during PPy coating.

The chemical composition of the AP-LMCN and PPy-LMCN was analyzed by ICP-AES. As Table 1 shows, the experimental composition of the AP-LMCN was in good agreement with the nominal composition, but the Li content in the PPy-LMCN decreased from 1.210 to 1.156 during PPy coating. This is attributed to the weak corrosion effect of the acidic hydrolyzed $FeCl_3$ on the solid solution. In the acidic condition, there is an $H^+ \leftrightarrow Li^+$ ion exchange and dissolution reaction occurs on the surface of the material [20].

$$LiMO_2 + H^+ \rightarrow HMO_2 + Li^+ \quad (1)$$

where $M = Li_{0.2}Mn_{0.54}Co_{0.13}Ni_{0.13}$.

The morphologies of the $Li_{1.2}Mn_{0.54}Co_{0.13}Ni_{0.13}O_2$ before and after 2.0 wt% PPy coating were shown in Fig. 2. The particle size of both samples is small and uniform ranging between 100 and 200 nm (Fig. 2a and b). The surface of the AP-LMCN particle is smooth. PPy coating makes the surface rough, indicating that the PPy covering is on the surface of $Li_{1.2}Mn_{0.54}Co_{0.13}Ni_{0.13}O_2$ particles. The distribution of the PPy coating layer on the surface was

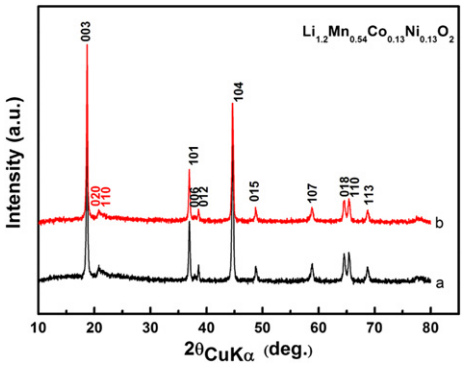

Fig. 1. X-ray diffraction patterns of (a) the as-prepared and (b) the PPy-coated $Li_{1.2}Mn_{0.54}Co_{0.13}Ni_{0.13}O_2$.

Table 1
The real contents of Li, Ni, Mn and Co (normalized to the Mn content) in the precursor of as-prepared and PPy-coated $Li_{1.2}Mn_{0.54}Co_{0.13}Ni_{0.13}O_2$.

	Li	Mn	Co	Ni
Precursor sample	1.200	0.540	0.130	0.130
Fired sample (800 °C)	1.210	0.540	0.130	0.124
PPy-coating sample	1.156	0.540	0.130	0.124

examined by energy dispersion spectroscopic (EDS) mapping of nitrogen (Fig. 2c and d). It can be inferred that the PPy distribution is uniform on the surface of $Li_{1.2}Mn_{0.54}Co_{0.13}Ni_{0.13}O_2$.

Fig. 3 displays the TEM images of the AP-LMCN (Fig. 3a), PPy-LMCN (Fig. 3b and c) and that of the 4.8 V charged PPy-LMCN (Fig. 3d). Bright and dark zones of a few nanometers wide are observed in Fig. 3a. These bands correspond to the inter-planar spacing of the (003) plane that is perpendicular to the $[001]_{hex}$. In each band, there are fringes with a space width of 4.7 Å. The edge of the PPy-LMCN particle is covered with a thin layer of amorphous species. In contrast, well-defined fringe patterns are observed in the inner of the PPy-LMCN particles (Fig. 3b and c). Based on the EDS mapping results, this amorphous species is attributed to the PPy coating layer on the $Li_{1.2}Mn_{0.54}Co_{0.13}Ni_{0.13}O_2$ particles. Continuous and uniform coating layer is not formed on the $Li_{1.2}Mn_{0.54}Co_{0.13}Ni_{0.13}O_2$ particle because the coating layer by the chemical oxidation polymerization is not sufficiently thick.

When the PPy-LMCN is charged to 4.8 V, a compact and uniform layer of amorphous species is obtained on the surface of the $Li_{1.2}Mn_{0.54}Co_{0.13}Ni_{0.13}O_2$ particle. Considering the rigidness and electrochemical inertness of the PPy coating layer, it is believed that electrolyte decomposition occurs and its products deposit to fill the discontinuous points of the PPy coating layer. However, the fringes remain clear and unchanged until the edge of the AP-LMCN particles when it is charged to 4.8 V (inset of Fig. 3d). This does not agree with the previous report in which the SEI layer was claimed to exist on the 4.8 V charged material without showing any evidence [8].

Fig. 4 compares the FTIR spectra of pure PPy and the PPy-LMCN charged to 4.8 V. As the positions of all the recognized bands are far from the characteristic bands of the solvents (EC at 1477, 1394, 1226, 1164, 1069, 970 cm^{-1} and DMC at 1757, 1456, 1276, 973, 915 and 795 cm^{-1}), the salt $LiPF_6$ of the electrolyte and the PPy coating layer, these observed bands are attributed to the decomposition products of the electrolyte rather than its residuals. Based on previous reports, these bands are assigned to the C═O stretch (1723, 1637 cm^{-1}) [21,22], CH_2 or CH_3 (1403, 1279, 1246, 880, 841 cm^{-1}) [21,22], C–O stretch (1183 cm^{-1}) [21,22], C–O–C stretch (1072 cm^{-1}) [21,22], and Li_2CO_3 (1435 cm^{-1}). Therefore, Li_2CO_3 and $R–OCO_2Li$ are supposed to be the main components of the deposition layer on 4.8 V charged PPy-LMCN, very similar to those of the SEI layer on other cathode materials at the charged states ($LiCoO_2$ charged to 4.5 V or over [23], for example). As a result, the SEI layer on the charged PPy-LMCN are expected to have similar electrochemical properties to that on those charged cathode materials. Indeed, the formation of this amorphous layer does not worsen the subsequent cycling performance of the material. This suggestion is supported with the following electrochemical impedance spectroscopic (EIS) characterization.

Fig. 5 shows the voltage profiles in the first cycle of the $Li_{1.2}Mn_{0.54}Co_{0.13}Ni_{0.13}O_2$ before and after surface modification. We noted that for both the AP-LMCN and the PPy-LMCN, an initial sloping region is followed by a plateau region at *ca.* 4.5 V. The slope corresponds to the oxidation of $Ni^{2+} \rightarrow Ni^{4+}$and $Co^{3+} \rightarrow Co^{4+}$ while the plateau was usually attributed to the irreversible loss of oxygen from the lattice [24]. Armstrong et al. [25] believed that the high-potential plateau region involves the loss of oxygen from the

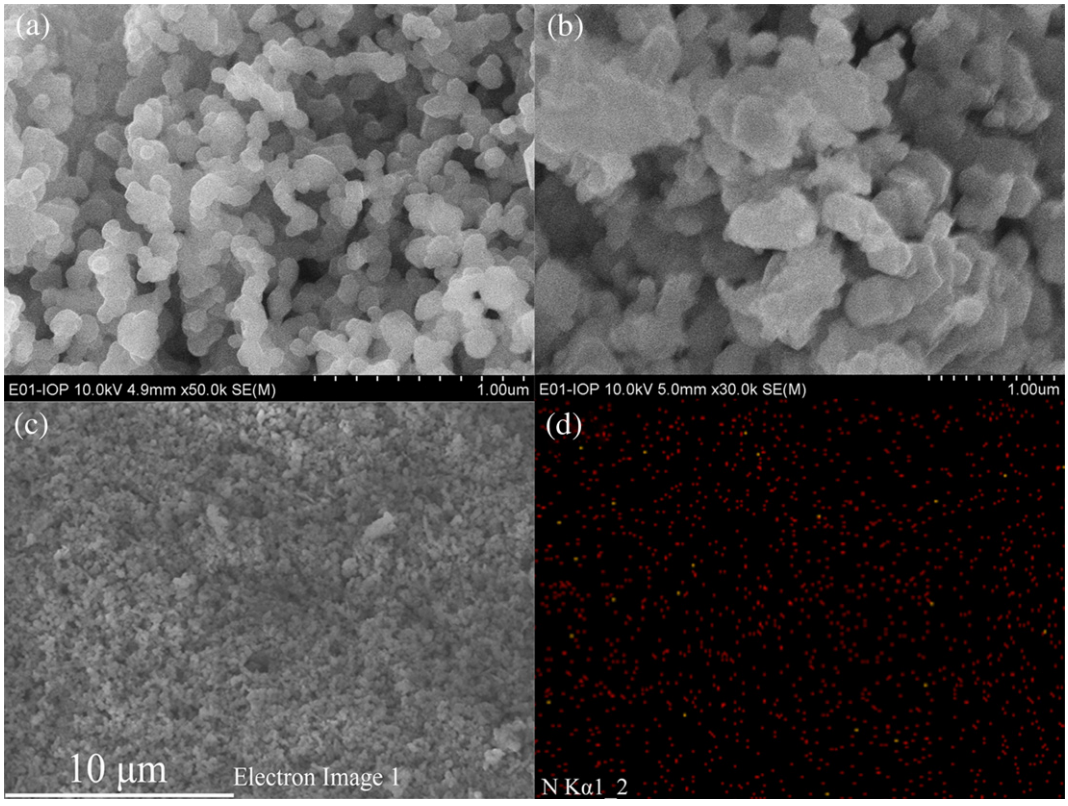

Fig. 2. The SEM images of the as-prepared (a) and 2.0 wt% PPy-coated (b and c) $Li_{1.2}Mn_{0.54}Co_{0.13}Ni_{0.13}O_2$. (d) Is the EDS mapping pattern of (c).

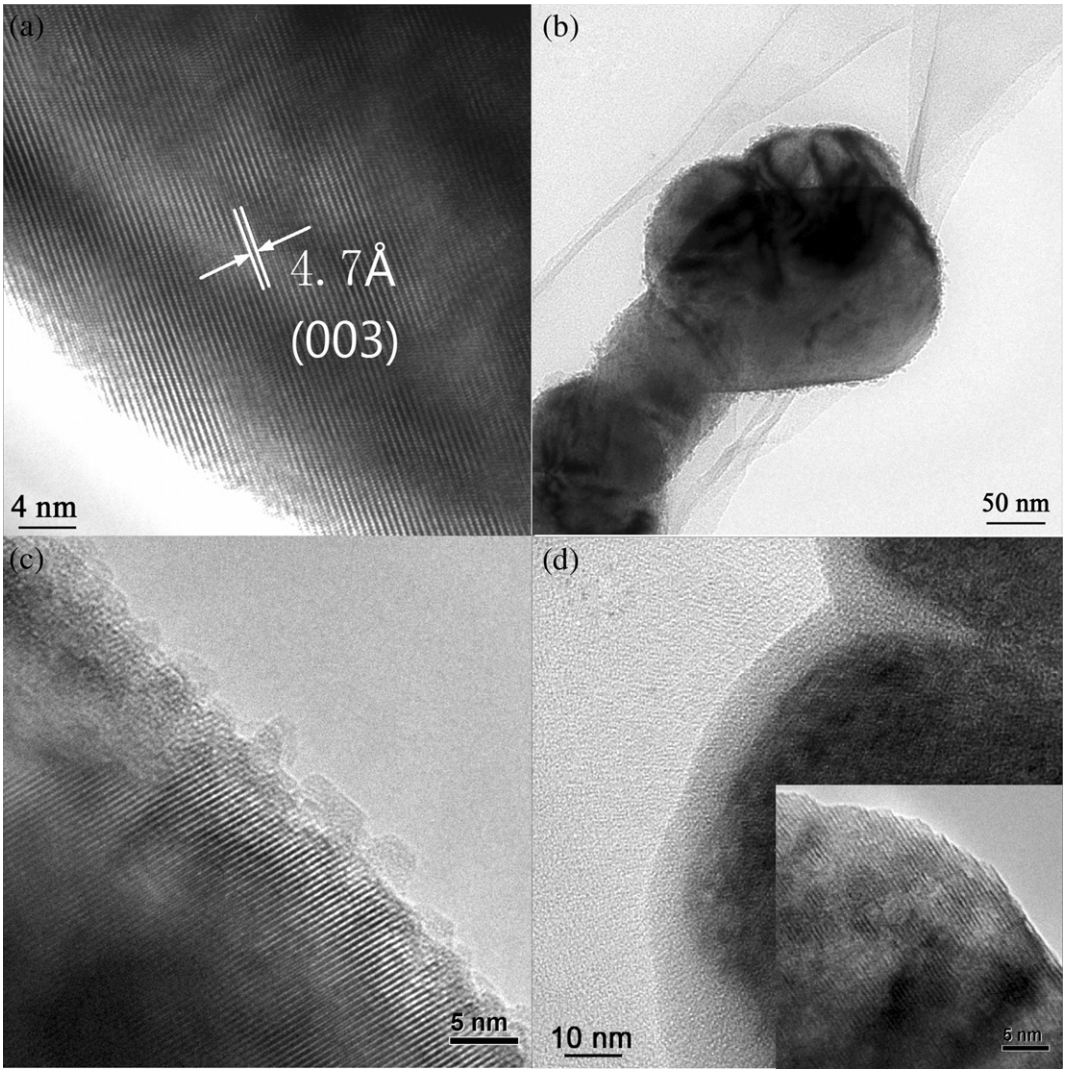

Fig. 3. The TEM images of the as-prepared (a) and PPy-coated (b and c) $Li_{1.2}Mn_{0.54}Co_{0.13}Ni_{0.13}O_2$. (d) Is the TEM image of the PPy-coated $Li_{1.2}Mn_{0.54}Co_{0.13}Ni_{0.13}O_2$ charged to 4.8 V; the inset is the TEM image of the as-prepared $Li_{1.2}Mn_{0.54}Co_{0.13}Ni_{0.13}O_2$ charged to 4.8 V.

surface in the form of Li_2O, followed by cationic and anionic diffusions to produce MO_2 (M = transition metal) with no oxygen ion vacancies left in the lattice. Loss of oxygen leads to the activation of oxidation states of Mn at the end of the initial charge.

The galvanostatic cycling further shows that although the initial charge capacity of PPy-LMCN is lower than that of the AP-LMCN (301 *vs.* 347 mAh g^{-1}), their discharge capacities are almost the same (267 mAh g^{-1} for the naked and 273 mAh g^{-1} for the coated). Although the loss of lithium ions during PPy coating (1.210 for AP-LMCN *vs.* 1.156 for PPy-LMCN) may be responsible for the difference of their charge capacities ($\sim$10–15 mAh g^{-1}), the main reason

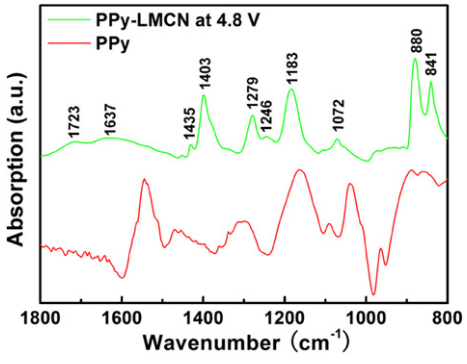

Fig. 4. FTIR spectra of the PPy and 2.0 wt% PPy-coated $Li_{1.2}Mn_{0.54}Co_{0.13}Ni_{0.13}O_2$ charged to 4.8 V.

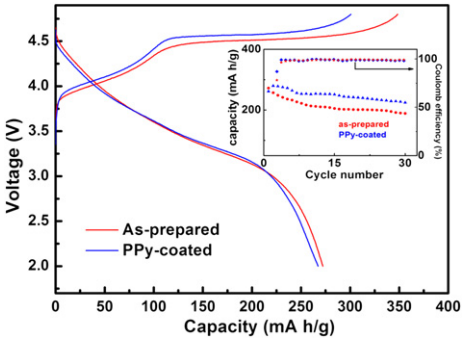

Fig. 5. Comparison of the first charge–discharge curves of $Li_{1.2}Mn_{0.54}Co_{0.13}Ni_{0.13}O_2$ before and after surface modification with PPy between 2.0 and 4.8 V at a current density of 12.5 mA g^{-1}. The inset is for their cycling performances and coulombic efficiencies.

for the capacity difference is definitely due to the suppression of electrolyte oxidation at high charge potentials (~30–35 mAh g^{-1}) because the PPy layer separates the active material from the electrolyte. It is understandable that the discharge capacity of the PPy-LMCN is slightly lower than the AP-LMCN because PPy is electronically conductive but insulating to the Li^+ ions. The presence of PPy does not facilitate the Li^+ ion transport at the surface of the solid solution, resulting in polarization of the cell as shown in the voltage profiles (Fig. 5). Anyway, surface modification suppresses the electrolyte decomposition and enhances the initial coulombic efficiency of the $Li_{1.2}Mn_{0.54}Co_{0.13}Ni_{0.13}O_2$ cathode material.

The cycling performances of the AP-LMCN and the PPy-LMCN are compared in the inset of Fig. 5. It is noted that the discharge capacities of both samples decrease with cycling. As the coulombic efficiency of both samples increases and becomes actually the same after the 2nd or 3rd cycle, the PPy coating layer are believed to take its function of suppressing the electrolyte decomposition only in the first few cycles. Slight electrolyte decomposition might remain in the subsequent cycles because the coulombic efficiency does not reach 100% even after quite a number of cycles as the cell is charged to 4.8 V. Therefore, the improved capacity retention of the PPy-LMCN is believed to be related to the suppression of the elimination of the oxygen vacancies and lithium insertion sites in the material. In addition, the discharge capacity of the PPy-LMCN increases from 262 mAh g^{-1} in the 1st cycle to 280 mAh g^{-1} in the 2nd cycle. This can be attributed to the insertion of some lithium ions into the Li^+ vacancies created during PPy coating, when some Li^+ ions were dissolved.

Fig. 6 compares the cyclic voltammograms of the AP-LMCN and PPy-LMCN between 2.0 and 4.8 V *vs.* Li^+/Li. In the initial sweep, two oxidation processes occur at 4.41 V and above 4.60 V, respectively, in the AP-LMCN (Fig. 6a). The 4.41 V peak is attributed to the lithium extraction from the $Li_{1.2}Mn_{0.54}Co_{0.13}Ni_{0.13}O_2$ lattice and the concomitant oxidation of the Co and Ni ions. The sharp 4.60 V peak

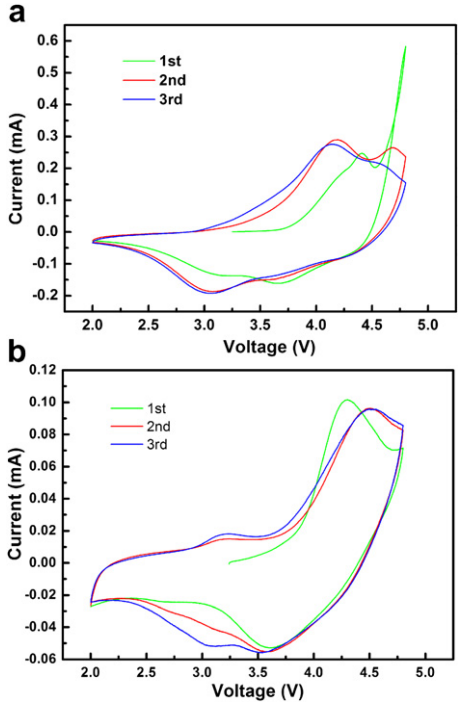

Fig. 6. Cyclic voltammograms of $Li_{1.2}Mn_{0.54}Co_{0.13}Ni_{0.13}O_2$ before (a) and after (b) PPy coating between 2.0 and 4.8 V at 0.1 mV s^{-1}.

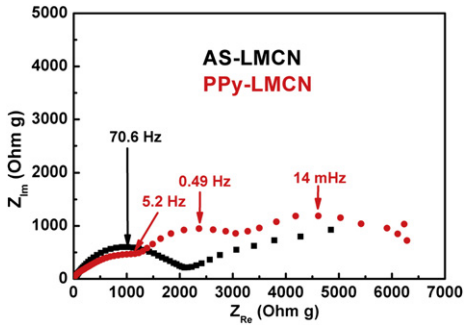

Fig. 7. Comparison of the electrochemical impedance spectra of the as-prepared (a) and PPy-coated (b) $Li_{1.2}Mn_{0.54}Co_{0.13}Ni_{0.13}O_2$ charged to 4.8 V *vs.* Li^+/Li.

is attributed to the electrolyte oxidation as well as the removal of Li_2O. The electrolyte oxidation is significantly suppressed after PPy coating because the strong and sharp oxidation peak disappears in the PPy-LMCN (Fig. 6b). This agrees with the improved coulombic efficiency of the surface modified sample (Fig. 5) and confirms the suppression of the electrolyte decomposition on the PPy layer. It was reported [26] that the reduction of Mn will be activated during the process of oxygen loss in the first cycle. A reduction peak is observed at 3.0 V in all the three reduction segments of the CV of the AP-LMCN, corresponding to the redox of Mn^{3+}/Mn^{4+}. A similar peak is not observed in PPy-LMCN until the 3rd cycle (Fig. 6b). This is evidence that oxygen release is suppressed to a great deal after PPy coating.

Fig. 7 compares the Nyquist plots of the LMCN before and after PPy coating. One semicircle plus a large arc are observed in the AP-LMCN while three semicircles are contained in the EISs for the PPy-LMCN in the frequency region. The semicircle for the AP-LMCN can clearly be attributed to the charge transfer within the LMCN, whereas the three semicircles for the PPy-LMCN correspond to the lithium diffusion in the SEI layer, lithium diffusion in the PPy layer, and charge transfer resistance (in the order from high to low frequency). It is difficult to determine if the large arc in the AP-LMCN be regarded as an imperfect semicircle (corresponding to lithium diffusion in the SEI layer) or just a slope (for solid state lithium diffusion into the layered oxide [27]) due to insufficiently low frequency of the EIS device, 4 mHz. However, considering the absence of the SEI layer as illustrated in the TEM (Fig. 3) and FTIR (Fig. 4), we prefer to take the arc as a slope. In addition, comparison of the mid-frequency semicircle of the PPy-LMCN and the single semicircle in the AP-LMCN indicates that PPy coating lowers the charge-transfer resistance of the material.

4. Conclusion

Layer-structured $Li_{1.2}Mn_{0.54}Co_{0.13}Ni_{0.13}O_2$ solid solution has been prepared and surface-modified with 2.0 wt% conducting polypyrrole. It is found that PPy coating improves the initial coulombic efficiency and the cycling stability of the material by suppressing the electrolyte decomposition and oxygen vacancy elimination at high potentials. In addition, the presence of the solid electrolyte interphase is confirmed on the PPy-coated $Li_{1.2}Mn_{0.54}Co_{0.13}Ni_{0.13}O_2$. Li_2CO_3 and $R-OCO_2Li$ are supposed to be the main components of the SEI layer on PPy-coated $Li_{1.2}Mn_{0.54}Co_{0.13}Ni_{0.13}O_2$.

Acknowledgment

The authors are thankful to National 973 Program of China (2009CB220100) and the National Natural Science Foundation of China (NSFC No. 20974120) for financial supports.

References

[1] J.M. Tarascon, M. Armand, Nature 414 (2001) 359–367.
[2] L. Croguennec, J. Bains, M. Ménétrier, A. Flambard, E. Bekaert, C. Jordy, P. Biensan, C. Delmas, J. Electrochem. Soc. 156 (2009) A349–A355.
[3] S.-H. Kang, M.M. Thackeray, J. Electrochem. Soc. 155 (2008) A269–A275.
[4] S.-H. Kang, Y.K. Sun, K. Amine, Electrochem. Solid-State Lett. 6 (2003) A183–A186.
[5] S.-H. Kang, K. Amine, J. Power Sources 124 (2003) 533–537.
[6] J. Jiang, K.W. Eberman, L.J. Krause, J.R. Dahn, J. Electrochem. Soc. 152 (2005) A1879–A1889.
[7] Y. Wu, A.V. Murugan, A. Manthiram, J. Electrochem. Soc. 155 (2008) A635–A641.
[8] J. Liu, Q.Y. Wang, B. Reeja-Jayan, Electrochem. Commun. 12 (2010) 750–753.
[9] Y. Wu, A. Manthiram, Electrochem. Solid-State Lett. 9 (2006) A221–A224.
[10] J. Liu, B. Reeja-Jayan, A. Manthiram, J. Phys. Chem. 114 (2010) 9528–9533.
[11] J.M. Zheng, Z.R. Zhang, X.B. Wu, Z.X. Dong, Z. Zhu, Y. Yong, J. Electrochem. Soc. 155 (2008) A775–A782.
[12] J.M. Zheng, J. Li, Z.R. Zhang, X.J. Guo, Y. Yong, Solid State Ionics 179 (2008) 1794–1799.
[13] S.Y. Chew, Z.P. Guo, J.Z. Wang, J. Chen, P. Munroe, S.H. Ng, L. Zhao, H.K. Liu, Electrochem. Commun. 9 (2007) 941–946.
[14] B.K. Guo, Q.Y. Kong, Y. Zhu, Y. Mao, Z.X. Wang, M.X. Wan, L.Q. Chen, Chem. Eur. J. 17 (2011) 14878–14884.
[15] G.X. Wang, L. Yang, Y. Chen, J.Z. Wang, S. Bewlay, H.K. Liu, Electrochim. Acta 50 (2005) 4649–4654.
[16] C.Q. Feng, S.Y. Chew, Z.P. Guo, J.Z. Wang, H.K. Liu, J. Power Sources 174 (2007) 1095–1099.
[17] H.B. Wang, Y.Q. Zeng, K.L. Huang, S.Q. Liu, L.Q. Chen, Electrochim. Acta 52 (2007) 5102–5107.
[18] P.X. Zhang, L. Zhang, X.Z. Ren, Q. Yuan, J.H. Liu, Q.L. Zhang, Synth. Met. 161 (2011) 1092–1097.
[19] C.S. Johnson, N.C. Li, C. Lefief, J.T. Vaughey, M.M. Thackeray, Chem. Mater. 20 (2008) 6095–6106.
[20] M.M. Thackeray, S.H. Kang, C.S. Johnson, J.T. Vaughey, R. Benedek, S.A. Hackney, J. Mater. Chem. 17 (2007) 3112–3125.
[21] D. Lin-Vien, N.B. Colthup, W.G. Fateley, J.G. Grasselli, Library of Congress Cataloging-in-Publication Data: The Handbook of Infrared and Raman Characteristic Frequencies of Organic Molecules, Academic Press, Inc., Boston, 1991.
[22] K. Nakanishi, P.H. Solomon, Infrared Absorption Spectroscopy, second ed., Holden-Day, Inc, San Francisco, 1977.
[23] Z.X. Wang, X.J. Huang, L.Q. Chen, J. Electrochem. Soc. 150 (2003) A199–A208.
[24] Y. Wu, A. Manthiram, Solid State Ionics 180 (2009) 50–56.
[25] A.R. Armstrong, M. Holzapfel, P. Novak, C.S. Johnson, S.-H. Kang, M.M. Thackeray, P.G. Bruce, J. Am. Chem. Soc. 128 (2006) 8694–8698.
[26] Z.H. Lu, J.R. Dahn, J. Electrochem. Soc. 149 (2002) A815–A822.
[27] Y. Huang, J. Chen, J. Ni, H. Zhou, X. Zhang, J. Power Sources 188 (2009) 538–545.